Nigerian Research Journal of Engineering and Environmental Sciences 5(1) 2020 pp. 239-252

Nigerian Research Journal of Engineering and Environmental Sciences
Journal homepage: www.rjees.com

Original Research Article

Influence of TIG Process Parameters on the Microstructure and Hardness Property of AISI 430 Ferritic Stainless Steel Welds using Response Surface Methodology Approach

***Musa, A.A., Dauda, E.T. and Bello, K.A.**
Department of Metallurgical and Materials Engineering, Ahmadu Bello University, PMB 1045, Zaria, Nigeria.
*abdulrahman@abu.edu.ng

ARTICLE INFORMATION

Article history:
Received 15 Dec, 2019
Revised 02 Mar, 2020
Accepted 04 Mar, 2020
Available online 30 June, 2020

Keywords:
Microhardness
Grain growth
Heat input
Microstructure
TIG welding technique

ABSTRACT

In the present study, the effect of tungsten inert gas (TIG) welding process parameters on microstructural features and hardness property of AISI430 ferritic stainless steel welds was investigated using response surface methodology, based on the central composite design (CCD). The process parameters considered in this study were the welding current (I), welding speed (S) and argon flow rate (AFR). It was observed that all input variables considered had direct influence on the microstructure as well as the hardness property of the weldment. Microstructural results indicate ferrite structures with finely dispersed particles aligned in the cold rolling direction for the base metal. The microstructure of the weld metal with the optimized conditions revealed the presence of martensite structures along the grain boundaries as well as fine equiaxed grains within the fusion and heat affected zones of the weldment. The welding speed plays the major role on the hardness property followed by the welding current and the argon flow rate in that order. An empirical model was generated from the obtained response to predict the weld quality in terms of the hardness value. An optimized hardness of 307.10 HV was predicted at the welding current of 22 A, welding speed of 5 mm/sec and argon flow rate of 10 L/min. Confirmation test was performed to check the practicability of the developed model and the results obtained was in good agreement with the predicted value with average percentage error of 2.21% which is within the acceptable value for adequate model.

1. INTRODUCTION

The tungsten inert gas (TIG) welding is increasingly being used as a suitable technique for welding different materials as well as surface treatment of steel alloy components (Bello *et al,* 2015). It is broadly utilized for joining alloy steels, stainless steels as well as repair and maintenance in various fabrication industries such as construction of bridges, ships, offshore structures, boilers, storage tanks, pressure vessels, pipelines,

automobiles, and railroad vehicles. (Vijayan and Seshagiri, 2018). Under the same welding conditions, TIG welding processes can produce improved mechanical properties as compared to gas metal arc welding (GMAW) processes (Ganesh *et al.*, 2014; Ugla, 2018). It offers minimum heat energy input with a high-quality clean weldment. Different metals inherently possess different weldability. Some metals are readily weldable, but some are difficult to weld, which require specific welding procedures (Mallaiah *et al.*, 2012).

Ferritic stainless steel (FSS) is a class of stainless steels with body-centered cubic crystal structure (BCC) having chromium content usually in the range of 11–27wt% (Balasubramanian *et al.*, 2008). These steels have good resistance to stress corrosion cracking (SCC), pitting corrosion and crevice corrosion particularly in aggressive environments (Sanjay *et al.*, 2018). They exhibit good ductility, formability, and moderately better yield strength relative to those of the austenitic grades, but the high temperature strength has been reported to be poor (Amuda and Mridha, 2011). One major problem that limits the industrial application of FSS is the loss of properties such as strength, hardness and impact toughness in the weld section due to the intense welding heat that induces grain coarsening (Lokesh *et al.,* 2015). Katundi *et al.*, (2010) reported that grain growth in the fusion zone (FZ) and heat affected zone (HAZ) occur due to high temperatures gradient experienced by the component during welding. It may be possible to improve the strength and the toughness of a fusion welded FSS if refined grain structure is produced in the microstructure (Amuda and Mridha, 2010).

Therefore, the present study investigates the influence of TIG process parameters on the microstructure and hardness properties of AISI 430 FSS welds using response surface methodology (RSM) approach.

2. MATERIALS AND METHODS

2.1. Sample Preparation

AISI430 ferritic stainless steel sheet with dimensions of 1200 mm (L) x 300 mm (W) x 1.5 mm (T) was selected for this study. It was purchased from Cenco Sains Company, Malaysia. The chemical composition of the stainless steel is given in Table 1.

Table 1: chemical composition of AISI 430 ferritic stainless steel (Amuda and Mridha, 2010)

Element	C	Si	Mn	P	S	Cr	Fe
% composition	0.12	0.75	1.00	0.040	0.030	17	81.06

2.2. Response Surface Methodology

Response surface methodology based on central composite design (CCD) was used to plan and design the experiment. The factors were varied over five levels (-α, -1,0, +1, +α) with three elements as factorial points, axial/star point and center runs. The factorial levels chosen for the current are 15 A and 25 A, while the values of 3 mm/s and 5 mm/s as well as 6 L/min and 10 L/min were selected for the speed and the argon flow rate respectively. The input factors and their levels are presented in Table 2.

Table 2: Factors and levels for the CCD experimental design plan

Factors	Symbols	Levels				
Welding current (A)	*A*	10	15	20	25	30
Welding speed (mm/s)	*B*	2	3	4	5	6
Argon flow rate (L/min)	*C*	4	6	8	10	12

2.3. TIG Torch Welding

Clarke 101 Inverter TIG welding setup shown in Figure 1 was selected for the welding of FSS in this investigation. In this process, direct current electrode negative (DCEN) also known as straight polarity was used for the autogenous TIG welding. The TIG welding machine used non-consumable tungsten electrode which contain 2% thorium and 2.5mm tip diameter. Pure argon gas was used as the shielding gas at a variable flow rates with the help of flow meter.

Figure 1: TIG welding machine setup

The sample (AISI 430 FSS) in sheet form with thickness 1.5 mm was cut into a dimension of 120 mm x 90 mm using cutting machine. It was then cut into two equal parts along the width and then butt weld using TIG welding process. After welding, test samples were cut from each of the welded plates for the determination of hardness properties and microstructural analysis.

2.3.1. Hardness testing

Hardness tests were performed using Vickers Microhardness testing machine. The samples were passed through metallographic preparation in order to obtain flat and smooth surface for regular indentation (Bello *et al.*, 2015). Each of the prepared test samples was then placed on an anvil that has a screw thread base as shown in Figure 2(b). The indenter was then pressed into the sample by an accurately controlled test force which was maintained between 10-15 seconds. The indentation was repeated three times on each sample in order to obtain the average hardness. The hardness test specimens from the welded samples were shown in Figure 2(a).

Figure 2(a): Hardness test specimen

Figure 2(b): Vickers microhardness tester

2.3.2 Microstructural analysis

Microstructural examination was carried out on the welded samples and the base metal by using optical microscope to reveal the microstructural changes due to heat energy input. After welding, the samples for investigation were prepared in accordance with the standard of the microscopic machine. The samples were first mounted in moulds with epoxy resin for easy handling prior to grinding and polishing operation. The mounted samples were then passed through grinding operation using different grit papers, starting from the rough (220 grit) to the finer grit (1200 grit) so that all scratches from cutting/sectioning can be removed. During grinding process, the direction of the samples was changed at right angle when moving from the previous grit to the next finer grit paper. This was to eliminate all the damages produced from the previous papers and also maintain the microstructural integrity of the specimen. The samples were then polished using a rotating polishing machine covered with a compound of alumina as the polishing cloth. The samples were moved around the rotating wheel until a mirror-like surface were achieved for each of the samples. Finally, they were etched in 50% Acetic-Nital-HCl to reveal the microstructure to be investigated. The setup was then loaded into the column of the microscopic machine which is connected to the monitor in a closed loop for which control and feedback are actualized as shown in Figure 3

Figure 3: Optical microscope

2.4. Experimental Design Matrix and Measured Response

Circumscribed central composite (CCC) design with three factors at five levels was chosen for the experimental design, and this represent the case of second-order modeling for the responses. The total number of experimental runs is estimated using $2^k + 2k + 6$, with 8 factorial points (2^k), 6-star points (2k) and 6 central runs to make up a total of 20 experimental runs, i.e. $2^3 + 2(3) + 6 = 8+6+6 = 20$ runs.

k is the number of input factors, and the central run is chosen as six (6) for convenience and accuracy especially when the input factors are more than two.

The factors with their levels and the responses were entered in the CCC design of the Design-Expert version 10 to generate the overall matrix for the analysis as shown in Table 3.

Table 3: Design matrix and responses for process parameters of TIG welding process

Experimental Run	Factors			Response
	Welding current (A)	Welding speed (mm/s)	Argon flow rate (L/min)	Hardness (HV)
1	15	3	10	268
2	20	4	8	321
3	20	4	8	315
4	15	5	10	283
5	15	3	6	233
6	25	3	10	270
7	20	4	8	305
8	20	6	8	320
9	10	4	8	210
10	25	3	6	315
11	20	4	12	300
12	20	2	8	262
13	20	4	8	328
14	30	4	8	266
15	15	5	6	305
16	25	5	6	347
17	20	4	8	340
18	25	5	10	300
19	20	4	8	290
20	20	4	4	327

3. RESULTS AND DISCUSSION

3.1. Regression Analysis of the Model for Hardness

The fit summary statistics analyses the relationship between the independent variables and the response by the regression analysis in order to fit all the models to the selected responses. The highest order polynomial with significant term for the hardness has F-value of 15.01 at $P < 0.0005$ as presented in Table 4 and the highest order of polynomial suggested by the model is the quadratic as indicated in the Table.

Table 4: Fit Summary statistics for the hardness model

Source	Sum of Squares	df	Mean Square	F Value	P-value Prob > F
Mean vs Total	1.755E+06	1	1.755E+06		
Linear vs Mean	11378.63	3	3792.88	4.04	0.0257
2FI vs Linear	2772.78	3	924.26	0.98	0.4315
Quadratic	10015.78	3	3338.59	15.01	0.0005
Cubic vs Quadratic	649.12	4	162.28	0.62	0.6660
Residual	1574.73	6	262.46		
Total	1.781E+06	20	89048.96		

3.2. Analysis of Variance (ANOVA) Test Results for the Hardness

The analysis of variance for the hardness with all the model terms is presented in Table 5. The model is significant having a p-value less than 0.05. The analysis of variance was carried out at 5% significance level or 95% confidence level. Equation 1 represents the model equation to predict the hardness based on the

process variable with significant model terms (A, B, C, AC, A^2 and B^2) as shown in Table 5. The model equation was developed from the analysis of variance. This model equation as presented in Equation 1 can be used to make predictions about the response for given levels of each factor. Here, the levels should be specified in the original units for each factor. However, the equation cannot be used to determine the relative impact of each factor because the coefficients are scaled to accommodate the units of each factor and the intercept is not at the center of the design space.

Table 5: Analysis of variance for the hardness

Source	Sum of squares	df	Mean square	F value	P-value Prob > F
Model	24157.37	7	3451.05	18.54	< 0.0001
A-Current	4715.23	1	4715.23	25.33	0.0003
B-Speed	5177.88	1	5177.88	27.82	0.0002
C-Argon flow rate	1485.52	1	1485.52	7.98	0.0153
AC	1994.91	1	1994.91	10.72	0.0067
BC	773.62	1	773.62	4.16	0.0641
A^2	9823.66	1	9823.66	52.78	< 0.0001
B^2	956.97	1	956.97	5.14	0.0426
Residual	2233.67	12	186.14		
Lack of Fit	697.12	7	99.59	0.32	0.9130
Pure Error	1536.55	5	307.31		
Cor Total	26391.05	19			

$$Hardness = -600.95857 + 46.95809x\ Current + 105.53295x\ Speed + 46.43219x\ Argon\ flow\ rate - 1.57913x\ Current\ x\ Argon\ flow\ rate - 4.91688\ x\ Speed\ x\ Argon\ flow\ rate - 0.77229\ x\ Current^2 - 6.02607x\ Speed^2 \quad (1)$$

The statistical summary presented in Table 6 is used to explain the amount of variability of the mean data. From the Table, the predicted R^2 of 0.7878 is in reasonable range of acceptance since the difference with the adjusted R^2 (0.8660) is less than 0.2. Also, the adequate precision of 18.154 which measures the signal to noise ratio also indicates an adequate signal which implies that the model can be used to navigate the design space since it is well above the required value of 4.0 suggested by the design expert.

Table 6: Summary of model statistics for hardness

Parameter	Value
R-Squared	0.9154
Adjusted R-Squared	0.8660
Predicted R-Squared	0.7878
Adequate Precision	18.154
Standard deviation	13.64
Mean	296.19
Coefficient of variation	4.61

3.3. Model Graphs for Hardness

The 3-D response surface graphs and contour maps for the hardness are presented in Figures 4 - 6. The input variables are shown in x and y axes while the response is presented on the z axis. Both the 3-D and the contour maps explain the effects of interactions between the variables on the hardness of the weldment. The graph shown in Figure 4 (a) and (b) represents the effect of the interaction between the current and the speed

on the hardness. From the 3-D surface plot and the contour map, it can be observed that hardness increases with increase in both the current and speed to about 330 HV and begin to drop as the current increases further above 25 A and speed above 5 mm/s. The hardness is minimum at a current of 10 A and a speed of 3 mm/s. The decrease in the hardness at lower current and speed was due to lack of proper weld penetration at lower current and speed. Hence, the interaction between current and the speed significantly influences the hardness of the weld (Navaneeswar and Venkata, 2018). Figure 5 (a) and (b) showed the influence of both current and the gas flow rate on the hardness property. It can also be observed from the graphs that the two input variables have positive effects on the hardness value of the welds. The hardness increases gradually from 200 HV to about 350 HV at a current of 26 A and a gas flow rate of about 5 L/min. However, as the current and the flow rate further increases to 30 A and 12 L/min respectively, the hardness dropped to about 250 HV as shown in Figure 5(b), this again, maybe due to too much heat input to the weld joint causing increase in the grain size, hence, reduces the hardness of the weldment (Amuda, and Mridha, 2012). The 3-D surface plot and the contour map shown in Figure 6 (a) and (b) respectively show the effects of interactions between the welding speed and the argon flow rate on the hardness value of the weldment. It is clearly observed from both plots that the hardness increases with increase in the welding speed and decreases with increase in the argon flow rate as shown by the blue and the red portion indicating higher and lower hardness value respectively. Maximum hardness of about 360 HV was obtained at a speed of 6 mm/s and gas flow rate of 4 L/min. As the gas flow rate increases to about 11 L/min and the speed is reduced to 3.3 mm/s, the hardness reduced to 300 HV as indicated in Figure 6(b). This variation is due to the fact that; higher welding speed usually requires high current in order to achieve the require penetration in the weld joint. However, if the gas flow rate is very high at high welding current, there may be too much oxidation at the welding zone which may reduce the hardness property of the weldment (Sharmistha and Neha, 2016).

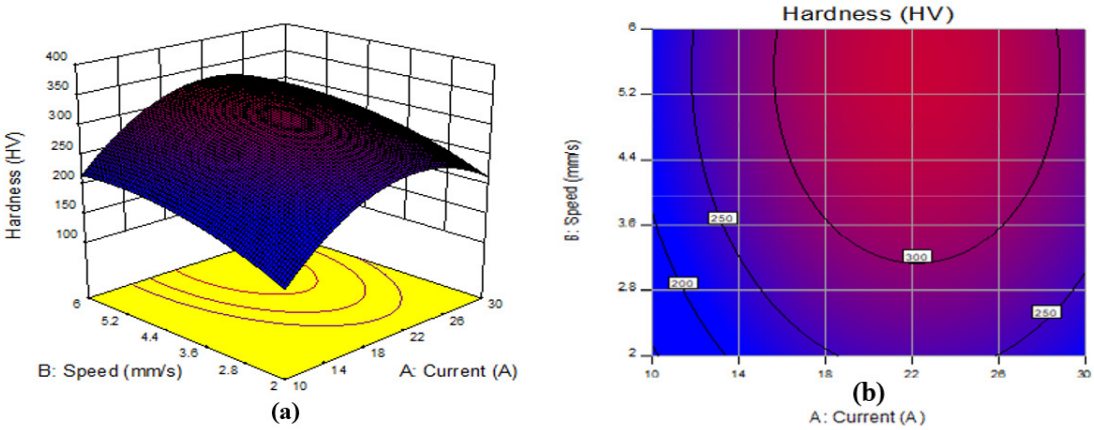

Figure 4: 3-D surface and contour plot showing the variation of hardness with welding current and speed (a) 3-D surface plot (b) contour plot

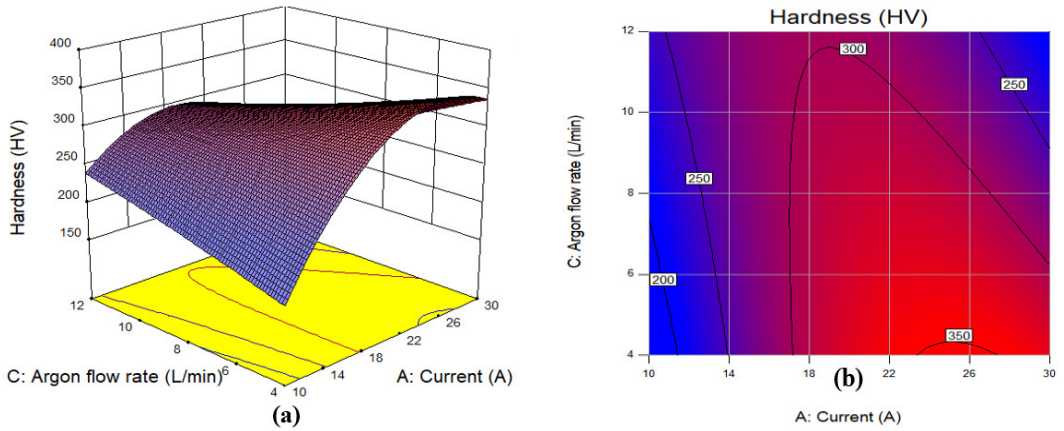

Figure 5: 3-D surface and contour plot showing the variation of hardness with welding current and the argon flow rate (a) 3-D surface plot (b) contour plot

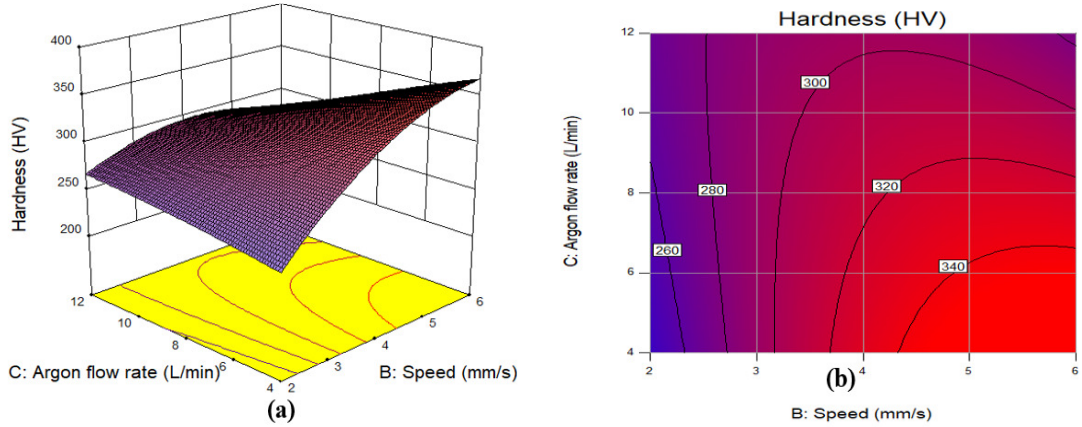

Figure 6: 3D surface and contour plot showing the variation of hardness with welding speed and the argon flow rate (a) 3-D surface plot (b) contour plot

3.4. Model Prediction Adequacy

The graph of predicted values against actual as shown in Figure 7 is important in order to evaluate the model capability. The data is expected to spread linearly along a straight line for the data to accomplish the model adequacy requirement according to the Design expert version 10 used. From the Figure, it is observed that the data clustered around a straight line indicating that the models are adequate for predicting the response within the experimental region.

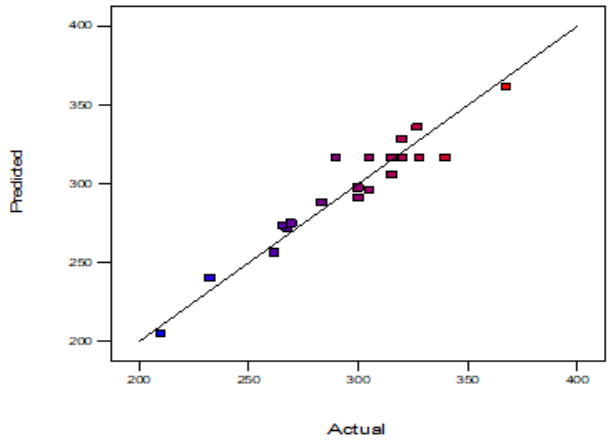

Figure 7: Plot of predicted against the measured values for hardness

3.5. Microstructural Analysis

The optical micrographs of some of the selected samples were shown in Figure 8(a-f). The selection of these weld samples for the microstructural investigation is based on the responses with maximum, minimum and average mechanical properties. It was observed that the quality of the weldment for all the samples is mainly controlled by the solidification behaviours of the weld metal. Also, the grain growth took place from the edge of the heat-affected zone (HAZ) to the fusion boundary in all the welded samples considered and some amount of martensitic structures were also found along the grain boundaries of the welds. It can be seen from the microstructures that the grains size and morphology were different in the fusion zone and heat affected zone as compared to base metal. Similar observations have been reported by Amuda and Mridha (2009). Figure 8(a) shows the micrograph of the base metal (as-received) having a fine-grained ferrite microstructure with finely disperse particles aligned in the cold rolling direction. Figure 8(b) shows the microstructure of the weld at a very low current (10 A) showing incomplete penetration with presence of some primary δ ferrite and some weld porosities within the matrix of the structure. This is due to low heat input into the weld joint thereby preventing the weld zone from proper fusion, leading to some micro porosities in the structure of the weldment (Buddu *et al.*, 2014). Figure 8(c) shows the microstructure of welds at 15 A, it can be observed from the microstructure that there is partial transformation of austenite at this moderate heat input due to fast cooling associated with the welds leading to little martensite formation at the grain boundaries as shown in the micrograph. As the current further increased, that is, increase in heat input rate the cooling rate is lower, allowing the elevated temperature delta ferrite transforms to ferrite and some austenite and reduce the martensite content (Razaullah *et al.*, 2016). These delta ferrite phases are the dark phases in the microstructure as shown in Figures 8d and 8e, the austenite then transforms to martensite as the weld cools to room temperature with some residual delta ferrite (Razaullah *et al.*, 2016). Also, Figures 8d and 8e indicate that the martensite is present along the ferrite grain boundaries as a continuous grain boundary phase in both the weld and the heat affected zone. At a very high current above 25A, the structure revealed the presence of intergranular precipitates as shown in Figure 8(f). These precipitates are formed as a result of supersaturation of carbon in the ferrite phase at elevated temperature which on cooling, the solubility of carbon in the ferritic stainless steel drops drastically from about 0.12wt % at 1395 ^{o}C to approximately 0.03 wt% at 1000 ^{o}C (Amuda and Mridha 2011).

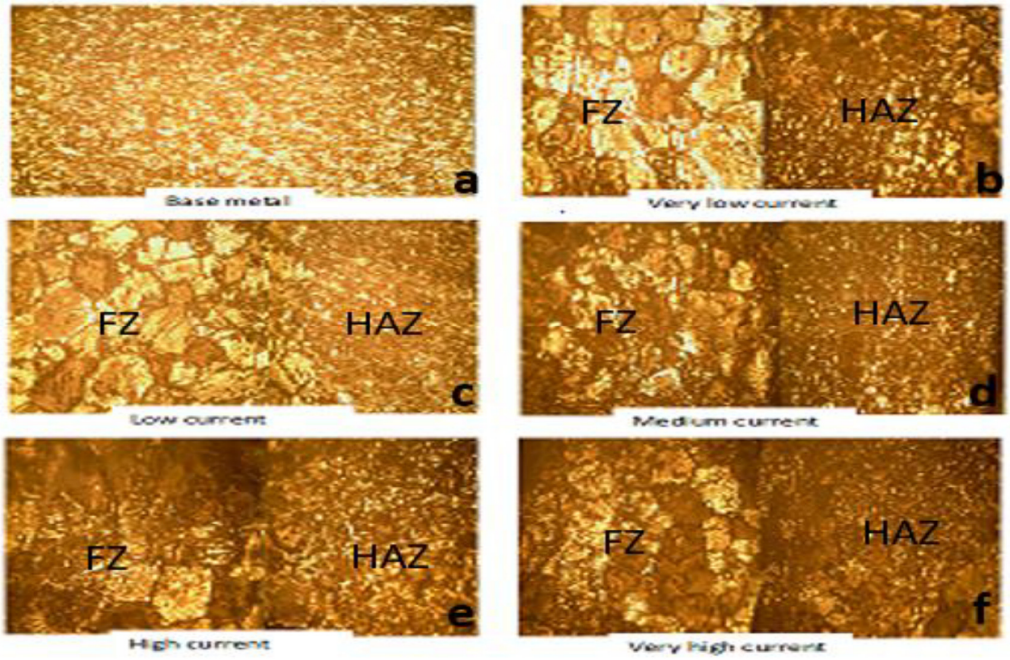

Figure 8: Micrographs of the base metal and welded metals (x100)

3.6. Analysis of the Micro-hardness

The distribution of the hardness across the weldment measured at 1.5mm intervals is presented in Figure 9. The hardness was measured in the longitudinal direction under different welding conditions. The weld specimen considered were grouped into four which include, welds at very low current, low current, medium current, high current and very high current based on the experimental design. It is observed from the Figure that the hardness values for all the samples considered followed the same trend. The fusion zone exhibits the highest hardness value and decreases gradually through the heat affected zone. This may be due to martensite formation at the fusion zone on solidification (Razaullah et al., 2016). It is also observed that hardness is higher at lower and intermediate heat input, this is related to the very rapid cooling rate which probably prevents excessive grain growth, which could have induced softening in the weldment thereby reducing the hardness values (Mallaiah *et al*., 2012). However, at a very high current (i.e. high heat input), the cooling rates is slower, since cooling rate is inversely proportional to the heat energy input. Therefore, the weld will spend more time to solidify leading to the formation of larger grains which give lower hardness value. Similar result was also reported by the study conducted by Amuda and Mridha (2011) on the effect of energy input on microstructure and hardness of TIG welded AISI 430 ferritic stainless steel. It was also observed from Figure 9 that, at a very low current, the hardness value further reduces, this could be attributed to the incomplete penetration of the welds, leading to lower properties (Buddu *et al.*, 2014).

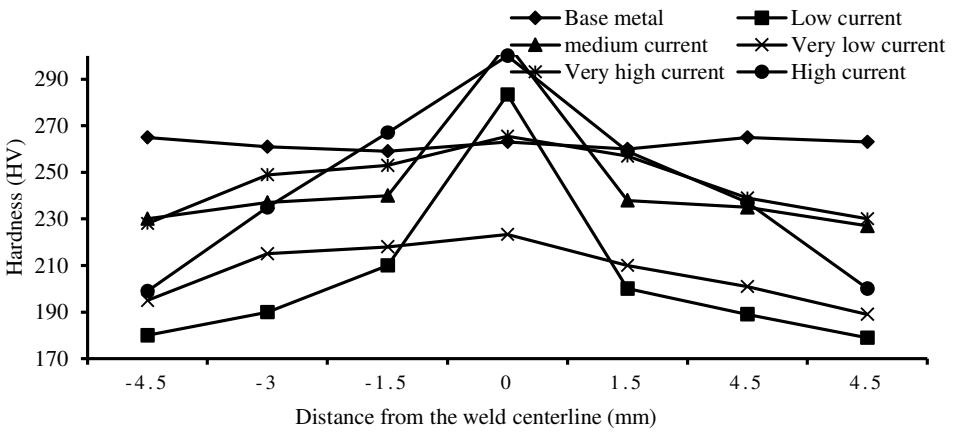

Figure 9: Longitudinal hardness profile across the weld section under different weld conditions

Figure 10 shows the influence of welding current on the hardness property of the optimized TIG ferritic stainless steel weld while keeping the other variables constant. This was obtained using the developed model equation of the hardness (Equation 1), and it is observed that the hardness increases gradually with increase in the welding current up to the optimum value of 22A and then decrease as the current further raised above the optimum value. This shows that the effect of current exhibits a parabolic trend on the hardness as shown in Figure 10. the decrease in the hardness at higher current is due to high energy input which induces coarse grains into the weld joint (Sharmistha and Neha, 2016). Also, current below the optimum value decreases the hardness value, this may be due to improper weld penetration, thereby creating porosities and undercut in the weldment with poor mechanical properties (Buddu *et al.*, 2014). Similar trend was also observed in Figure 11 where the hardness value was maximum at 5mm/s welding speed and decrease below and above the optimum value.

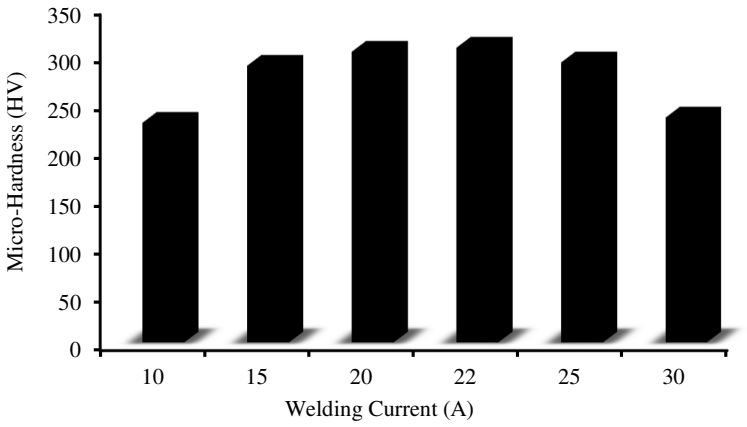

Figure 10: Influence of welding current on the micro-hardness for the optimized weld

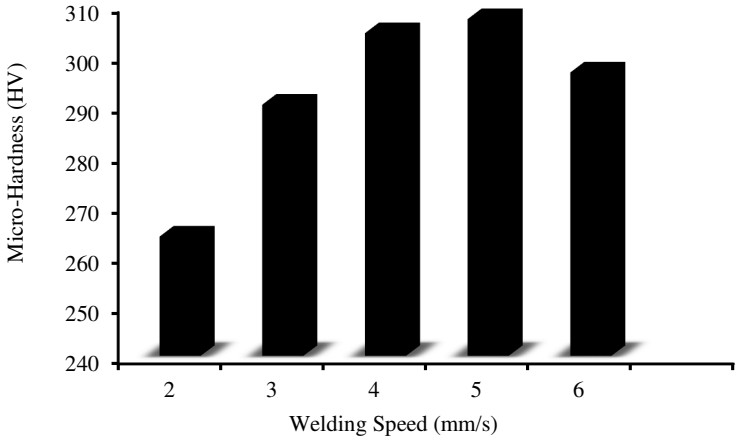

Figure 11: Influence of welding speed on the micro-hardness for the optimized welds

3.7. Confirmation Test Results

In order to validate the test results of optimization generated from the developed model, confirmatory tests were also performed using the predicted process parameters and compared with the predicted responses. Two confirmatory tests were performed as presented in Table 7 and the average percentage error was calculated. It can be observed from the Table that the predicted and observed results were in a good agreement with average percentage of 2.21% which is within the satisfactory range of percentage error (Vidyarthy *et al*. 2017).

Table 7: Confirmation test results

Test No.	Process parameter			Response		
	Current (A)	Speed (mm/s)	Argon flow rate (L/min)	Predicted	Observed	% Error
1	21.737	5	10	307.10	301.532	1.81
2	22.440	5	10	305.027	297.10	2.60

4. CONCLUSION

In this study, optimization of TIG process parameters on the hardness properties of AISI 430 ferritic stainless steel was investigated. The following conclusions were drawn from the present work.

1. Production of ferritic stainless steel welds was successfully achieved using TIG welding techniques.
2. The microstructural examination proved that there is grain growth in the weld and heat affected zone of the weldment.
3. The optimized input variables are welding current (22 A), welding speed (5 mm/s) and the argon flow rate (10 L/min) with the optimum output of 307.10 HV.
4. The welding speed appears to be the most influential parameter on the hardness value followed by the welding current and argon flow rate.
5. The confirmation experiment was successfully performed to validate the modeling and optimization of the process. The average percentage error was 2.21%, which is within the accepted range as per RSM design method.

5. ACKNOWLEDGEMENT

The authors wish to acknowledge the support of Ahmadu Bello University, Zaria -Nigeria, and the entire staff of the department of Metallurgical and Materials Engineering for their words of encouragement.

6. CONFLICT OF INTEREST

There is no conflict of interest associated with this work.

REFERENCES

Amuda, M.O.H. and Mridha S. (2010). Grain refinement in ferritic stainless steel welds: the journey so far. *Advanced Materials Research,* 83, pp. 1165-1172.

Amuda, M.O.H. and Mridha, S. (2009). Microstructural features of AISI 430 ferritic stainless steel (FSS) weld produced under varying process parameters. *International Journal of Mechanical and Materials Engineering* 4(2), pp.160-166.

Amuda, M.O.H. and Mridha, S. (2011). Effect of Energy Input on Microstructure and Hardness of TIG Welded AISI 430 Ferritic Stainless Steel. *Advanced Materials Research*, 264, pp. 390-396.

Amuda, M.O.H. and Mridha, S. (2012). Comparative evaluation of grain refinement in AISI 430 FSS by elemental powder addition and cryogenic cooling. *Materials and Design*, 35, pp. 609-618.

Balasubramanian, V., Shanmugan, K. and Lakshminarayanam, A.K. (2008). Effect of autogenous arc welding processes on fatigue crack growth behavior of ferritic stainless steel joints. *Iron and Steel Institute of Japan International*, 48(4), pp. 489–495.

Bello, K.A., Maleque, M.A., Ahmad, Z. and Mirdha, S. (2015). Optimization of Hardness Behaviour of TIG Modified Ceramic Coating Using the Taguchi Approach. *Advanced Materials Research*, 1115, pp. 238-242.

Buddu, R.K., Chauhan, N. and Raole, P.M. (2014). Mechanical properties and microstructural investigations of TIG welded 40 mm and 60 mm thick SS 316L samples for fusion reactor vacuum vessel applications. *Fusion Engineering and Design,* 12(89), pp. 3149 – 3158.

Ganesh, K.C., Vasudevan, M., Balasubramanian, K.R., Chandrasekhar, N. and Vasantharaja, P. (2014). Thermomechanical analysis of TIG welding of AISI 316LN stainless steel. *Materials Manufacturing Process,* 29, pp. 903-909

Katundi, D., Tosun-Bayraktar, A., Bayraktar, E. and Toueix, D. (2010). Corrosion behaviour of the welded steel sheets used in automotive industry. *Journal of Achievement in Materials and Manufacturing Engineering,* 38, pp. 146–153.

Lokesh, K.G., Karthikeyan, P., Narasimma, R.C., Prasanna, B. and George, O. (2015). Microstructure and Mechanical Properties of ASS (304)-FSS (430) Dissimilar Joints in IN SMAW and GTAW Process. *International Journal of Engineering Sciences and Research Technology*, 6, pp. 367-378.

Mallaiah, G., Kumar, A., Ravinder, P.R. and Madhusudhan, G. R. (2012). Influence of grain refining elements on mechanical properties of AISI 430 ferritic stainless steel weldments -Taguchi approach. *Materials and Design,* 36, pp. 443–450

Mridha, S. and Amuda, M.O.H. (2011). An Overview of Sensitization Dynamics in Ferritic Stainless Steel Welds. *International Journal of Corrosion,* 2011, pp. 1-9.

Navaneeswar, G.R. and Venkata, M.R. (2018). Optimization of process parameters in welding of dissimilar steels using robot TIG welding. *IOP Conf. Series: Materials Science and Engineering* 330, pp. 1-7

Razaullah K.M., Pathak, A.K., Umasankar, D. and Dhirendra, T. (2016). Study of Microstructure and Mechanical Properties of Feritic Stainless Steel (AISI 430) Weldment using ER309L and ER430 electrodes by MIG welding process. *International Journal of Engineering Research & Technology*, 5(1), pp. 312-318

Sanjay, K.G., Avinash, R.R., Meghanshu, V. and MohdZaheer, K.Y. (2018). Effect of heat input on microstructure and mechanical properties in gas metal arc welding of ferritic stainless steel. *Materials Research Express*, 6(3), pp. 1-17.

Sharmistha, S. and Neha, G. (2016). Analysis of Hardness in Metal Inert Gas Welding of Two Dissimilar Metals, Mild Steel & Stainless Steel. *IOSR Journal of Mechanical and Civil Engineering (IOSR-JMCE)*, 13(3), pp. 94-113.

Ugla, A.A. (2018). Enhancement of weld quality of AISI 304L austenitic stainless steel using a direct current pulsed TIG arc. *IOP Conference Series: Materials Science and Engineering*, 433, pp. 1-15.

Vidyarthy, R.S., Dwivedi, D.K. and Vasudevan, M. (2017). Optimization of A-TIG Process Parameters Using Response Surface. *Materials and Manufacturing Processes,* 33(7), pp. 1-31.

Vijayan, D. and Seshagiri, V.R. (2018). Process Parameter Optimization in TIG Welding of AISI 4340 Low Alloy Steel Welds by Genetic Algorithm. IOP Conf. Series: *Materials Science and Engineering,* 390**,** p. 012066.